Satellite derived shorelines at an exposed meso-tidal beach

Carlos Cabezas-Rabadán*, Josep E. Pardo-Pascual*, Jesús Palomar-Vázquez*, Óscar Ferreira**, Susana Costas**

*CGAT Research Group; Dept. Cartographic Eng. Geodesy and Photogrammetry: Universitat Politècnica de València; Valencia, Spain
**CIMA/FCT; Universidade do Algarve; Faro, Portugal

ABSTRACT

Shoreline position data offer extremely valuable information for understanding coastal dynamism and beach changes. This research applies SHOREX system for defining the shoreline position from free mid-resolution Landsat-8 (L8) and Sentinel-2 (S2) satellite imagery. This system allows an automatic definition of Satellite Derived Shorelines (SDS) over large regions and periods. Accuracy and utility of the resulting SDS have been previously assessed with positive results at low energy, microtidal, Mediterranean beaches. This work assesses SDS extracted using SHOREX at a mesotidal and moderate to highly (during storms) energetic environment, namely at Faro Beach, a barrier beach located in Ria Formosa (Algarve, South Portugal). Accuracy was defined for 14 SDS derived from S2 and 10 from L8 by measuring the differences in position with respect to the shoreline inferred from profiles obtained on close dates (or simultaneously) to imagery acquisition. For non-simultaneous datasets, the water level was estimated for the time of the satellite images acquisition using oceanographic data and run-up formulations. The measured and estimated shoreline positions were then compared with the extracted SDS. The overall accuracy is good, with errors about 5 m RMSE, supporting the application of the used methodology to define shoreline dynamics and evolution at challenging environments, as mesotidal exposed and dynamic beaches.

INTRODUCTION

Beaches are highly dynamic natural spaces, often facing sudden changes or long-term evolution trends, which can be strongly conditioned by anthropogenic pressure. Monitoring those changes is of paramount relevance to understand coastal evolution and potential hazards, as well as to define coastal management actions. The continuous acquisition of accurate shoreline position is of outmost importance for the monitoring of coastal areas. For this purpose, it is therefore essential to have efficient methodologies that correctly define and extract the shoreline position with low and known errors. Those methodologies can use traditional sources of information as aerial photography, GNSS, LiDAR, UAV and, more recently, video-monitoring (e.g. Sánchez-García *et al.*, 2017). All these sources of information allow recording the shoreline position with high precision but always with limitations inherent to the coverage and the frequency of data acquisition. Landsat-8 (L8) and Sentinel-2 (S2) medium resolution satellites offer free images quasi-continuously (one each 2.9 days combining both platforms, Li & Roy, 2017) and covering large coastal areas. Taking advantage of the differences in the land/water edge in IR (infrared) bands, several algorithms have emerged to obtain Satellite-Derived Shorelines. For the moment, only a few extraction methodologies have achieved subpixel accuracy (e.g. Liu *et al.*, 2017; Pardo-Pascual *et al.*, 2012; Song *et al.*, 2019; Viaña-Borja and Ortega-Sánchez, 2019; Vos *et al.*, 2019). Their assessments are very limited on real scenarios, as they require large sets of high-precision reference data. Thus, only few extraction methodologies have been tested on beaches, using for validation purposes aerial photographs (Viaña-Borja & Ortega-Sánchez, 2019), UAV (Palomar-Vázquez *et al.*, 2019), terrestrial photogrammetry (Pardo-Pascual *et al.*, 2018) and, more commonly, in-situ topographic profiles (e.g. Hagenaars *et al.*, 2018; Liu *et al.*, 2017; Vos *et al.*, 2019). SDS extracted with the system SHOREX (Palomar-Vázquez *et al.*, 2018) have been recently compared with simultaneous video extracted shorelines on Cala Millor beach (Sánchez-García *et al.*, 2020), reaching 3.57 m RMSE for L8 and 3.01 m for S2 imagery. Nevertheless, due to the nature of this Mediterranean beach, the assessment has been constricted to low energy conditions and an almost negligible tidal range. Extraction methodologies should be tested and improved for different types of coasts, facing a wider range of tides, waves and swash processes. Such improvement will allow a robust and validated acquisition of the SDS for the vast majority of coastal areas, as well as understanding the influence of the oceanographic processes on the location (and dynamism) of the shoreline.

This work aims to adapt, improve and validate the accuracy of SDS from L8 and S2 imagery using data from an exposed mesotidal beach in order to fill the current lack of assessments on different types of coasts. This would facilitate the applicability of the method to a wider range of coasts worldwide.

METHODS

Field site

The field work was conducted at Faro Beach, located in Ancão Peninsula, a relatively narrow sand barrier in Algarve, South Portugal. This exposed steep-beach commonly develops beach cusps and it is backed by a dune ridge (Figure 1). It is a mesotidal beach with semi-diurnal tides with an average range of 2.8 m for spring tides, and 1.3 m for neap tides. Annual significant offshore wave height is 0.92 m with 8.2 s of average peak period (Costa *et al.* 2001).

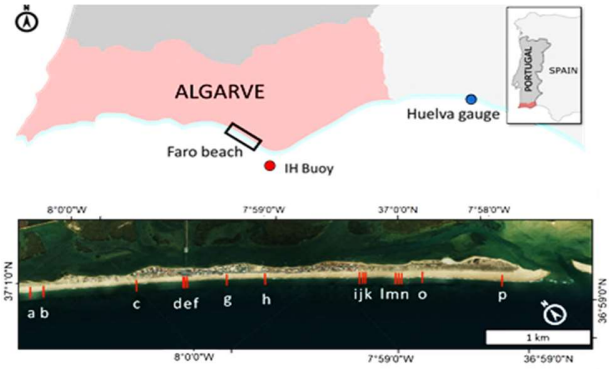

Figure 1. Location of the study area in Faro Beach, as well as the tide gauge and the wave buoy. Detail of the location of the topographic cross-shore profiles.

Field data

In-situ RTK-GNSS surveys were carried out 14 different days defining cross-shore profiles at 16 selected locations distributed over 4.5 km alongshore. A variable number of profiles (between 1 and 7) was used per date (see Figure 1, Table 1).

The position of the shoreline was estimated for each profile in order to be used as validation data. To do so, the total water level (considered as the run-up excursion) was determined as:

$$TWL = TL + SS + R \quad (1)$$

where TL is the tidal level, SS is the storm surge and setup, and R is the run-up (by incident waves). Sea level (TL + SS) was obtained from a tide gauge deployed at Huelva Harbor (Spanish Port Authorities, see Figure 1, Table 2), while offshore wave conditions were obtained from a buoy (Portuguese Hydrographic Institute, IH, Figure 1, Table 2) for the nearest possible conditions in relation to the satellite imagery acquisition. The sea level was corrected to the Portuguese vertical datum.

Table 1. *Date of the topographic surveys, used profiles per date, and associated satellite imagery.*

Sentinel-2	Landsat-8	GNSS survey	Profiles
19/07/2016	23/07/2016	22/07/2016	a, b, p, o
17/10/2016	11/10/2016	17/10/2016	a, b, p, o
15/01/2017	15/01/2017	15/01/2017	a, b, p, o
05/04/2017	05/04/2017	29/03/2017	a, b, p, o
09/07/2017	10/07/2017	07/07/2017	a, b, p, o
02/10/2017	28/09/2017	03/10/2017	p, o
11/11/2017	15/11/2017	09/11/2017	p, o
20/01/2018	18/01/2018	23/01/2018	b
19/02/2018	-	26/02/2018	c, d, e, f, g, h, p
05/04/2018	-	05/04/2018	b, c, d, e, f, g, p
25/04/2018	-	20/04/2018	c, d, e, f, g, h
15/05/2018	10/05/2018	17/05/2018	b, c, f, g, h
17/10/2018	17/10/2018	17/10/2018	i, j, k, l, m, n
21/11/2018	-	21/11/2018	i, j, k

Table 2. *Significant wave height (Hs), peak period (Tp) and Sea Level (SL=TL+SS) associated with the satellite imagery acquisition.*

Date	Satellite	Hs (m)	Tp (m)	SL (m)
19/07/2016	S2	1.18	7.5	0.89
23/07/2016	L8	0.65	8	-0.86
11/10/2016	L8	0.41	10	1.01
17/10/2016	S2	0.55	10.8	-0.02
15/01/2017	L8	1.41	6.2	-1.29
15/01/2017	S2	1.35	5.85	-1.16
05/04/2017	L8	1.08	14.3	0.79
05/04/2017	S2	1.03	13.8	0.73
09/07/2017	S2	0.53	6.6	0.41
10/07/2017	L8	0.48	11.8	-0.09
28/09/2017	L8	0.53	5.5	0.2
02/10/2017	S2	0.89	6.2	1.31
11/11/2017	S2	0.52	3.5	0.17
15/11/2017	L8	1	4.5	1.34
18/01/2018	L8	1.11	16.7	-0.42
20/01/2018	S2	0.6	13.8	-0.88
19/02/2018	S2	0.5	10.9	-0.97
05/04/2018	S2	1.11	13.32	-0.74
25/04/2018	S2	0.7	9.1	1.26
15/05/2018	S2	0.45	11.1	0.54
17/10/2018	L8	0.73	7	0.47
17/10/2018	S2	0.77	7.5	0.37
21/11/2018	S2	1.43	14	1.22

R was determined following the empirical formulation proposed by Vousdoukas *et al.* (2012):

$$R=0.58\ Ho\ \xi+0.46 \quad (2)$$

where R is the run-up, Ho is the deep water significant wave height, and ξ is the Iribarren number. This model was selected since it was developed specifically for Faro Beach. Since SDS do not necessarily reflect the maximum run-up excursion neither the starting of the swash, it was necessary to identify the run-up excursion that better represents the location of the extracted SDS. Thus, four test cases were analyzed: (i) the estimated run-up level, (ii) 2/3 of it, (iii) half of it, and (iv) 1/3 of it. TWL was defined according to these test cases, and the points of the profiles intersecting the respective TWL were identified as the estimated shoreline position (Figure 2). The estimation is sustained under the assumption of invariant beach profiles between the acquisition of GNSS and satellite data.

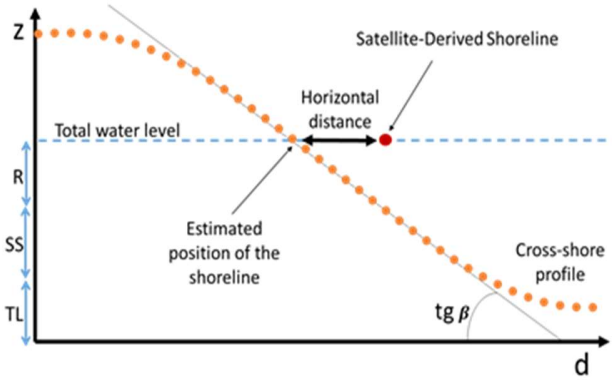

Figure 2. Scheme of a cross-shore profile defined by GNSS points with certain elevation (z) along distance (d). TWL is defined for the instant the SDS are acquired, and the point intersecting the profile constitutes the estimated position of the shoreline. The horizontal distance between the estimated position and SDS defines the error of the extracted shorelines.

Experimental data & accuracy assessment

Twenty-four mid-resolution S2 and L8 images were downloaded free of charge from Copernicus Open Access Hub and USGS explorer respectively (see Table 1). Covering the period 22 July 2016 - 21 November 2018, the selected images were the closest in time to the available GNSS surveys, with a maximum temporal mismatch of seven days and a percentage of clouds below 30%. The SDS was defined as the water/land intersection at the instant of the image acquisition. The extraction followed the workflow described by Palomar-Vázquez *et al.* (2018) using the SHOREX system. It applies the sub-pixel algorithmic solution proposed by Pardo-Pascual *et al.* (2012), and uses Short-Wave Infrared bands (SWIR1) and a third-degree polynomial in order to extract the shoreline from the kernels of analysis. An equivalent kernel size was defined for both satellites (7x7 and 5x5 pixels for S2 and L8 respectively), while a mask was used to cover the inner lagoon and focus the extraction on the desired interface.

SDS positions were horizontally compared against the estimated position of the shore over the GNSS profiles, employed as reference data for validation and error assessment (see Figure 2). Thus, SDS from S2 were compared against the estimated shorelines defined in up to 55 profiles while SDS from L8 were compared against up to 36 shoreline positions. The error was described for each run-up test case using: bias (average distance), precision (standard deviation, hereafter σ), and accuracy (RMSE).

RESULTS

Bias and accuracy registered by the SDS differed both in relation with the satellite source and the run-up test case considered (Table 3). On the contrary, precision values were similar for all the run-up test cases, being slightly lower for L8 (σ about 5.5 m) than for S2 (σ about 4.5 m). For both satellites, bias (and associated with that, the accuracy) changed remarkably when considering different partial values of the run-up proposed by the models. Bias showed a dominating seaward displacement of the SDS with the highest values when considering the total run-up level (test case i), with estimated shorelines displaced more than 6 m inland from the position of the SDS derived both from L8 and S2. The bias decreased for both satellites when considering 2/3 of the calculated run-up (case ii), and even more when considering half of it (case iii) (see Table 3). The smaller differences were obtained when considering 1/3 of the calculated run-up (case iv) being the bias landward directed. L8 presented, for all cases, a slightly smaller bias than S2.

Results suggest that accuracy is linked to the bias. Thus, for both satellites the highest accuracy occurs at test cases iii and iv, being higher for S2 (smaller value) than for L8.

Table 3. *Bias (average distance), precision (standard deviation), and accuracy (RMSE) for each satellite source and different run-up test cases (I to iv). Positive values show a landward displacement of the SDS. Values at bold highlight the best results.*

Satellite	Test case	i	ii	iii	iv
L8	no. profiles	35	36	36	36
	Bias (m)	-6.29	-3.05	-1.41	**0.12**
	Precision (m)	5.55	**5.47**	5.69	5.67
	Accuracy (m)	8.33	6.19	5.78	**5.77**
S2	no. profiles	55	49	44	42
	Bias (m)	-6.59	-3.25	-1.29	**0.53**
	Precision (m)	4.61	4.48	**4.44**	4.75
	Accuracy (m)	8.01	5.50	**4.58**	4.72

DISCUSSION

Despite the recent progress in shoreline extraction techniques, quality assessments using as reference in-situ data on beaches are scarce and often limited to low energy, microtidal coastal areas (e.g. Hagenaars *et al.*, 2018; Liu *et al.*, 2017; Pardo-Pascual *et al.*, 2018; Sánchez-García *et al.*, 2019, 2020; Vos *et al.*, 2019). When considering higher energy and meso-macrotidal beaches the comparison is mostly limited to a reduced number of points/profiles or hydrodynamic conditions (e.g. Vos *et al.*, 2019).

The present assessment of SDS extracted from both L8 and S2 satellites contributes to fill the general lack of in-situ tests in diverse coastal types. This work assesses SDS extracted with SHOREX using a relatively large data set (between 35 and 55 compared shorelines depending on the test case) obtained at an exposed mesotidal beach experiencing Hs up to 1.43 m and Tp over 14 s during the evaluation days. The accuracy for the extracted shorelines is about 5 m RMSE (Table 3). While bias showed a similar pattern in both satellites, precision was slightly higher in S2 (Table 3), being also translated to the values of accuracy. Nevertheless, it should be highlighted that the temporal difference between L8 images and the reference data was greater, potentially enhancing the inaccuracy. Under the most favorable run-up scenarios, results appeared in line with the preliminary test of SDS extracted with SHOREX at the energetic and microtidal Reñaca Beach, Central Chile. In that work, coincident shorelines derived from photogrammetric surveys were used as validation data, being the obtained accuracy of the SDS about 4.55 m RMSE for the combination of S2 and L8 (Sánchez-García *et al.*, 2019). Accuracy results are comparable to

those obtained in more robust assessments performed on Mediterranean beaches with low wave energy conditions and reduced tidal range. In those works, SDS extracted with SHOREX were compared against alongshore GNSS surveys on el Saler Beach, Spain (Pardo-Pascual *et al.*, 2018) and, more recently, against a large package of video monitored shorelines (91) on Cala Millor Beach, Balearic Islands (Sánchez-García *et al.*, 2020). This latter assessment defined accuracy values of 3.57 m and 3.01 RMSE for SDS derived from L8 and S2 imagery respectively. Nevertheless, that beach experiences almost negligible tides (below 0.25 m) and low waves (Hs usually below 0.9 m and Tp between 4 and 7 s). Those conditions contrast with the present assessment in Faro Beach, in which higher waves and especially longer peak periods may cause larger horizontal excursions.

When comparing with the assessments performed for other extraction methodologies, SHOREX seems to present good results even considering a mesotidal and moderately energetic coastal area, like Faro Beach. Hagenaars *et al.* (2018) assessed SDS from S2 and Landsat 5, 7 and 8 along 4.5 km of the microtidal Dutch coast (average tidal range of 1.7 m and mean Hs of 1.3 m). They reported average errors (expressed as average bias ± standard deviation) for L8 and S2 images of 9.5 (±16 m) and 10.5 (±12 m) respectively when filtering measurements associated with calm wave conditions (wave heights below 0.5 m) and 21.9 (±49 m) for S2 and 19.9 (±44 m) when no filters were applied. Liu *et al.* (2017) evaluated SDS from L5, L7 and L8 on the 3.6 km microtidal Narrabeen Beach, Australia (tidal range below 2 m, mean Hs and Tp of 1.6 m and 10 s respectively), and reported about 10 m RMSE when comparing full series of SDS, while annual mean shorelines were within 5.7 m RMSE. More recently, Vos *et al.* (2019) carried out tests on four microtidal beaches (Australia, New Zealand and USA) with accuracy values ranging from 7.2 m to 11.6 m RMSE. This same work also included a test on the meso-macrotidal Truc Vert Beach, France (3.7 m of mean spring tidal range and 1.4 m of Hs, using one single reference profile) with accuracy results of 12.7 m RMSE.

Oceanographic conditions and wave characteristics may act as important inaccuracy drivers during SDS extraction. Higher Hs and Tp are associated with higher run-up and larger excursions. Some authors have pointed out the existence of a relation between accuracy, the foam of the breaking waves and the wave period (Hagenaars *et al.*, 2018; Pardo-Pascual *et al.*, 2018). For a better assessment of shoreline definition accuracy from satellite imagery it is key to know which position of the beachface is being identified by the SDS. The instantaneousness of the image, together with the spatial and temporal oscillations of the shoreline resulting from the alternation of swash and backswash processes makes it difficult to tell. The image is a snapshot that often includes an alongshore undulated shoreline as a function of swash/backwash processes, and/or the existence of beach cusps or any other coastal undulations. The extracted SDS integrate different degrees of humidity or water inundation, not being easy to define the exact process or beach position they represent. The tests of the present study have allowed approaching the uncertainty about the exact location of the extracted shoreline on the beachface, contributing to understand what the extraction systems are actually mapping. The role of the swash on the shoreline definition has been evidenced as large differences appeared in the measured errors, depending on the values considered for the run-up. The lowest bias and the highest accuracy were reached when considering half and one third of the run-up level defined according to the empirical model proposed by Vousdoukas *et al.*, 2012 (Table 3, test case iii and iv). In fact, if a simple regression analysis is performed to the results, the zero bias is attained for a position representing 35-37% of the total run-up. These results seem to indicate that SDS represent a line following positions sometimes covered by the water sheet created by swash processes, and not necessarily a clear separation between wet/dry portions of the beach.

The definition, use and exploitation of SDS for coastal monitoring, already viable at Mediterranean beaches, require extra considerations when working on other types of coast. On the one hand, and with regard to the shoreline definition, the high variability experienced by the shoreline position on a beach like Faro Beach brings some requirements to the extraction workflow directly imposed by the specific characteristics of the studied zone. Thus, kernel sizes have been adapted (7x7 and 5x5 pixels for S2 and L8 respectively) based on previous tests (Pardo-Pascual et al., 2018; Sánchez-García *et al.*, 2020) in order to ensure an extraction process focused on the desired pixels. On the other hand, and with regard to the application of the extracted shorelines, an appropriate comparison of SDS from different dates makes it necessary to deal with the effect of variant oceanographic conditions. The knowledge of wave and tide data at the time of acquisition of the satellite images together with information on the beachface morphology may allow horizontal corrections of the SDS position, making compatible the use of shorelines of dates with different conditions. Once SDS accuracy is quantified for new environments, many applications can be potentially explored, as the characterization of mid-term (Almonacid-Caballer *et al.*, 2016) or decadal shoreline changes (Liu *et al.*, 2017). The availability of many individual shoreline positions may allow robust studies of coastal evolution for different time scales (days to decades), based on large data sets. Thus, SDS make it possible to define the beach state before and after impacts, either of natural origin, as storms (Pardo-Pascual *et al.*, 2014), or anthropogenic, as sand nourishments or coastal protection works (Cabezas-Rabadán *et al.*, 2019a,b).

CONCLUSIONS

This study constitutes the first assessment of SDS extracted using SHOREX on an exposed mesotidal coast, employing for this purpose a large dataset of oceanographic conditions and measured beach profiles. The accuracy (5.77 m and 4.58 m RMSE for L8 and S2 respectively) was in the same order of magnitude, or even slightly lower, than in previous assessments on microtidal Mediterranean beaches, and lower than in previous studies for other meso-macrotidal beaches. This is a very positive result considering that the test took place in an exposed beach with moderate Hs (up to 1.43 m) and long peak periods (up to 14 s). The validation of the accuracy of the SDS in more challenging coastal types widens the potential applications of

this extraction methodology, constituting a low-cost source of data with high spatial and temporal resolution helpful for studying the coast and monitoring beach changes.

ACKNOWLEDGMENTS

Authors appreciate the support of the Spanish Ministry of Economy and Competitiveness for the funds associated with the project RESETOCOAST (CGL2015-69906-R). C. Cabezas-Rabadán contribution was funded by the Spanish Ministry of Education, Culture and Sports (FPU15/04501). Ó. Ferreira contribution was funded by EW-COAST (PTDC/CTA-OHR/28657/2017) and by the Portuguese Science and Technology Foundation (FCT) through the grant UID/MAR/00350/2013 attributed to CIMA of the University of Algarve. The contribution of S. Costas was funded by the contract IF/01047/2014. Authors also thank the Portuguese Hydrographic Institute (IH) for supplying oceanographic data in collaboration with CIMA.

LITERATURE CITED

Almonacid-Caballer, J., Sánchez-García, E., Pardo-Pascual, J. E., and Balaguer-Beser, A. Palomar-Vázquez, J., 2016. Evaluation of annual mean shoreline position deduced from Landsat imagery as a mid-term coastal evolution indicator. *Marine Geology*, 372, 79-88.

Cabezas-Rabadán, C., Pardo-Pascual, J. E., Almonacid-Caballer, J., and Rodilla, M., 2019a. Detecting problematic beach widths for the recreational function along the Gulf of Valencia (Spain) from Landsat 8 subpixel shorelines. *Applied Geography*, 110.

Cabezas-Rabadán, C., Pardo-Pascual, J. E., Palomar-Vázquez, J. M., and Fernández-Sarría, A., 2019b. Characterizing beach changes using high-frequency Sentinel-2 derived shorelines on the Valencian coast (Spanish Mediterranean). *Science of the Total Environment*, 691, 216-231.

Costa, M., Silva, R. and Vitorino, J., 2001. Contribuição para o estudo do clima de agitação marítima na costa portuguesa. *In: 2as Jornadas Portuguesas Engenharia Costeira e Portuária. International Navigation Association*

Hagenaars, G., de Vries, S., Luijendijk, A. P., de Boer, W.P., and Reniers, A.J., 2018. On the accuracy of automated shoreline detection derived from satellite imagery: A case study of the sand motor mega-scale nourishment. *Coastal Engineering*, 133, 113-125.

Li, J. and Roy, D.P., 2017. A global analysis of Sentinel-2a, Sentinel-2b and Landsat 8 data revisit intervals and implications for terrestrial monitoring. *Remote Sensing*, 9(902).

Liu, Q., Trinder, J.C., and Turner, I.L., 2017. Automatic super-resolution shoreline change monitoring using Landsat archival data: A case study at Narrabeen–Collaroy Beach, Australia. *Journal of Applied Remote Sensing*, 11(1), 016036.

Palomar-Vázquez, J.M., Almonacid-Caballer, J., Pardo-Pascual, J.E., Cabezas-Rabadán, C., and Fernández-Sarría, A., 2018. Sistema para la extracción masiva de líneas de costa a partir de imágenes satélite de resolución media para la monitorización costera: SHOREX. *In:* López-García, M.J, Carmona, P., Salom., and Albertos, J.M (eds.), *Proceedings: XVIII congreso TIG*, pp. 25-35.

Palomar-Vázquez, J., Pardo-Pascual, J.E., Cabezas-Rabadán, C., and Alonso-Aransay, D., 2019 Monitorizando los cambios de superficie y volumen de la Laguna de Gallocanta mediante imágenes Landsat-8 y Sentinel-2. *In:* Durán, R., Guillén, J., and Simarro, G. (eds.), *Proceedings: X Jornadas de Geomorfología Litoral* pp. 205-208.

Pardo-Pascual, J.E., Almonacid-Caballer, J., Ruiz, L.A., and Palomar-Vázquez, J., 2012. Automatic extraction of shorelines from Landsat TM and ETM+ multi-temporal images with subpixel precision. *Remote Sensing of Environment* 123, 1–11.

Pardo-Pascual, J. E., Almonacid-Caballer, J., Ruiz, L. A., Palomar-Vázquez, J., and Rodrigo-Alemany, R., 2014. Evaluation of storm impact on sandy beaches of the Gulf of Valencia using Landsat imagery series. *Geomorphology*, 214, 388-401.

Pardo-Pascual, J.E., Sánchez-García, E., Almonacid-Caballer, J., Palomar-Vázquez, J.M., de los Santos, E.P., Fernández-Sarría, A., and Balaguer-Beser, A., 2018. Assessing the accuracy of automatically extracted shorelines on microtidal beaches from Landsat 7, Landsat 8 and Sentinel-2 imagery. *Remote Sensing* 10.

Sánchez-García, E., Balaguer-Beser, A., and Pardo-Pascual, J.E., 2017. C-Pro: A coastal projector monitoring system using terrestrial photogrammetry with a geometric horizon constraint. *ISPRS Journal of Photogrammetry and Remote Sensing*, 128, 255-273.

Sánchez-García, E; Briceño, I., Palomar-Vázquez, J., Pardo-Pascual, J., Cabezas-Rabadán, C., Balaguer-Beser, Á., 2019. Beach Monitoring Project on Central Chile. *In: 5ª Conferência MEC2019*

Sánchez-García, E., Palomar-Vázquez, J. M., Pardo-Pascual, J. E., Almonacid-Caballer, J., Cabezas-Rabadán, C., Gómez-Pujol, L. 2020. An efficient protocol for accurate and massive shoreline definition from mid-resolution satellite imagery. Coastal Engineering, 103732.

Song, Y., Liu, F., Ling, F., and Yue, L., 2019. Automatic Semi-Global Artificial Shoreline Subpixel Localization Algorithm for Landsat Imagery. *Remote Sensing*, 11(15), 1779.

Viaña-Borja, S. P., and Ortega-Sánchez, M., 2019. Automatic Methodology to Detect the Coastline from Landsat Images with a New Water Index Assessed on Three Different Spanish Mediterranean Deltas. *Remote Sensing*, 11(18), 2186

Vousdoukas, M. I., Wziatek, D., and Almeida, L. P., 2012. Coastal vulnerability assessment based on video wave run-up observations at a mesotidal, steep-sloped beach. *Ocean Dynamics*, 62(1), 123-137.

Vos, K., Harley, M. D., Splinter, K. D., Simmons, J. A., and Turner, I. L., 2019. Sub-annual to multi-decadal shoreline variability from publicly available satellite imagery. *Coastal Engineering*, 150, 160-174.